

# Baryogenesis and Dark Matter with Vector-like Fermions

M. Fairbairn<sup>1</sup> and P. Grothaus<sup>2</sup>

*Theoretical Particle Physics and Cosmology Group  
Physics Department  
King's College London  
London WC2R 2LS  
UK*

October 29, 2018

## Abstract

We show that vector-like fermions can act as the dark matter candidate in the universe whilst also playing a crucial role in electroweak baryogenesis through contributing to the barrier in the one-loop thermal scalar potential. In order for the new fermions to give rise to a strong first order phase transition, we show that one requires rather large Yukawa couplings in the new sector, which are strongly constrained by electroweak precision tests and perturbativity. Strong couplings between the dark matter candidate and the Higgs boson intuitively lead to small values of the relic density and problems with dark matter direct detection bounds. Nevertheless, when considering the most general realisation of the model, we find regions in the parameter space that respect all current constraints and may explain both mysteries simultaneously.

## 1 Introduction

The recent discovery of the (Brout-Englert-Kibble-Guralnik-Hagen) Higgs boson at the LHC [1,2] has led to a new surge in research concerning its possible implications for beyond the Standard Model physics.

At the same time, we know from galaxy rotation curves, clusters, lensing and structure formation both in galaxies and within the plasma before the last scattering surface that the Universe seems to contain about five times as much dark matter (DM) as matter. So far there is no information from the LHC which elucidates the nature of this mysterious component.

Furthermore, even though there is evidence for CP-violation in the Standard Model (see e.g. [3,4]), it is not clear what is the explanation for the fact that there is more matter than anti-matter in the Universe. While a source of CP-violation is an essential ingredient for this asymmetry, we also require some form of out-of-equilibrium physics in order to ensure that any baryon asymmetry is not washed out [5]. Baryon number violating processes are known to exist

---

<sup>1</sup>malcolm.fairbairn@kcl.ac.uk

<sup>2</sup>philipp.grothaus@kcl.ac.uk

in the Standard Model [6, 7], but the question of how to achieve a strong enough deviation from thermal equilibrium is still a matter of discussion. This can be achieved by heavy particles decaying out of equilibrium [8, 9] or through strong first order electroweak phase transitions [10].

At the time of writing the couplings of the new boson to the rest of the Standard Model seem to confirm that it does indeed behave in the way that one would expect from a Standard Model Higgs boson [11–13]. However, there is still some uncertainty with regards to the branching ratios for the decay channels of the Higgs, in particular, the situation for the  $h \rightarrow \gamma\gamma$  channel has not yet been clarified. Whereas the ATLAS experiment still observes a slight excess in that channel [14], the CMS experiment finds a value completely consistent with the Standard Model expectation [15]. It is clear that one of the key tasks in the immediate program of the LHC will be to test these couplings as they may show evidence of coupling to other particles beyond the Standard Model.

One simple expansion of the Standard Model that could explain such a deviation is vector-like fermions, i.e. fermions whose left and right handed components transform in the same way under the Standard Model gauge groups. Past works have demonstrated that not only can vector-like fermions enhance the diphoton rate, but also that there are possible connections to other phenomena such as dark matter or baryogenesis. (For recent works on vector-like fermions, see for example [16–37]). In this paper we will examine these connections in greater detail - in particular we aim to explore the compatibility of an explanation of both dark matter and baryogenesis within one single set-up of vector-like fermions and see how future measurements in the diphoton channel affect these links.

Given the value of the Higgs boson and the mass of the top quark, it appears at the time of writing that the running of the quartic coupling of the Higgs is such as to render the electroweak vacuum metastable [38–40]. Generically at one loop, bosons make the beta function of the quartic coupling more positive while fermions make it more negative. The addition of vector-like fermions to the theory will consequently make this problem more acute and demands new physics to appear at some higher scale which we will not speculate on in this work. A possible solution would be supersymmetric versions of vector-like fermions, as investigated in for example [27, 29, 30, 33].

The rest of the paper is organised as follows: In section 2 we will present the Lagrangian and the mass matrices of the model and write down the quantum numbers of the theory. In section 3 we will describe the steps involved in looking for parameters of the Lagrangian that provide viable dark matter candidates and a strong electroweak phase transition without creating modifications to the propagation of Standard Model particles which would have already been detected. We then go on to present the results in section 4 before discussing our conclusions.

## 2 Lagrangian and Mass Matrices

In this work we investigate the model proposed in reference [18]. We will use the exact same notation here in order to avoid unnecessary confusion and present in this section the Lagrangian and resulting mass matrices. Note that such a model may arise by gauging lepton number, as explained in references [16, 31, 32].

The model consists of a  $SU(2)$  doublet  $\ell'_L$  with Standard Model type couplings as well as corresponding singlets  $e'_R$  and  $\nu'_R$  plus, to make it vector-like, mirrored fields with opposite chirality. See also table 1 for clarification of the different fields and their quantum numbers. The

Field	$\ell'_L, \ell''_R$	$e'_R, e''_L$	$\nu'_R, \nu''_L$
$SU(3) \times SU(2) \times U(1)$	$(1, 2, -1/2)$	$(1, 1, -1)$	$(1, 1, 0)$

Table 1: The new fields and their  $SU(3) \times SU(2) \times U(1)$  quantum numbers.

Lagrangian is given by

$$\begin{aligned} \mathcal{L} = & \mathcal{L}_{\text{SM}} - m_\ell \bar{\ell}'_L \ell''_R - m_e \bar{e}''_L e'_R - m_\nu \bar{\nu}'_L \nu'_R - \frac{1}{2} m' \overline{\nu}'_R{}^c \nu'_R - \frac{1}{2} m'' \overline{\nu}''_L{}^c \nu''_L \\ & - Y'_c (\bar{\ell}'_L H) e'_R - Y'_n (\bar{\ell}'_L \tau H^\dagger) \nu'_R - Y''_c (\bar{\ell}''_R H) e''_L - Y''_n (\bar{\ell}''_R \tau H^\dagger) \nu''_L + \text{h.c.} \end{aligned} \quad (1)$$

Here, the symbol  $\tau$  represents the antisymmetric  $2 \times 2$  matrix in  $SU(2)$  space with non zero components  $\tau_{12} = 1$  and  $\tau_{21} = -1$ . There are therefore nine free parameters of the model - five masses and four Yukawa couplings. With  $v = 246$  GeV one obtains the following mass matrices for the charged sector

$$\left( \overline{e}'_L \ \overline{e}''_L \right) \mathcal{M}_c \begin{pmatrix} e'_R \\ e''_R \end{pmatrix} + \text{h.c.} \quad \text{with} \quad \mathcal{M}_c = \begin{pmatrix} \frac{Y'_c v}{\sqrt{2}} & m_\ell \\ m_e & \frac{Y''_c v}{\sqrt{2}} \end{pmatrix}, \quad (2)$$

and for the neutral sector

$$\frac{1}{2} \left( \overline{\nu}'_L \ \overline{\nu}'_R{}^c \ \overline{\nu}''_R{}^c \ \overline{\nu}''_L \right) \mathcal{M}_n \begin{pmatrix} \nu'_L{}^c \\ \nu'_R \\ \nu''_R \\ \nu''_L{}^c \end{pmatrix} + \text{h.c.} \quad \text{with} \quad \mathcal{M}_n = \begin{pmatrix} 0 & \frac{Y'_n v}{\sqrt{2}} & m_\ell & 0 \\ \frac{Y'_n v}{\sqrt{2}} & m' & 0 & m_\nu \\ m_\ell & 0 & 0 & \frac{Y''_n v}{\sqrt{2}} \\ 0 & m_\nu & \frac{Y''_n v}{\sqrt{2}} & m'' \end{pmatrix}. \quad (3)$$

These matrices are diagonalised such that we obtain the masses and mixings of the physical states. The charged sector requires two independent unitary matrices  $U_L$  and  $U_R$ , whereas one unitary matrix  $V$  is sufficient for the neutral sector. In this analysis we will use the symbols  $N_{1,2,3,4}$  and  $E_{1,2}$  for the mass eigenstates of the neutral and charged fermions, respectively. Their masses will be written as  $M_{N_{1,2,3,4}}$  and  $M_{E_{1,2}}$  and their couplings to the Higgs boson as, e.g.,  $C^{N_1 N_1 h}$  or  $C^{E_1 E_1 h}$ .

Now we will go on to show how we investigate different numerical values for the free parameters in the model. Although there is a very large nine-dimensional parameter space, this will be considerably reduced by requiring the model to not only give rise to a viable DM candidate, but also to trigger a first order phase transition, to keep modifications to the electroweak precision variables small (as observed) and to give an excess in the diphoton rate.

### 3 Methodology

In this section we will outline the procedure for the different tests we perform on a given set of parameters to see if they are compatible with dark matter, baryogenesis, electroweak precision variables etc. In the next section we will present the results of this analysis.

### 3.1 Parameter Ranges and Diagonalisation

Since we investigate the complete accessible nine-dimensional parameter space, we rely on the diagonalisation routines from the SLHApplus package [41] to find the mass eigenstates and mixing matrices of the new charged and the neutral vector-like fermions. For this we use Singular Value Decomposition and Takagi Decomposition respectively. The resulting lightest neutral state will then be our dark matter particle  $N_1$  with a mass  $m_{\text{DM}}$ . As we expect the expressions for the masses and mixing elements to be too complicated to be illuminating, we perform the complete work without considering analytic expressions.

Our parameter ranges are given as follows:

$$\begin{aligned} m' &\in [0, 4000] \text{ GeV}, & m'' &\in [0, 4000] \text{ GeV}, & m_\ell &\in [0, 4000] \text{ GeV}, \\ m_\nu &\in [0, 4000] \text{ GeV}, & m_e &\in [0, 4000] \text{ GeV}, & Y'_c &\in [0, 3.6], \\ Y''_c &\in [0, 3.6], & Y'_n &\in [0, 3.6], & Y''_n &\in [0, 3.6]. \end{aligned}$$

The upper limits on the mass parameters are set to 4 TeV as we do not expect any changes for even heavier mass parameters, as we would enter the decoupling regime more and more. We implement perturbativity by setting an upper limit on the Yukawa couplings of 3.6.

### 3.2 Electroweak Constraints

In order to ensure that the additional particles do not create problems for the successful predictions of the Standard Model, we need to check that the quantum corrections they induce upon the propagators of the W and Z bosons are not too large. These corrections are usually parameterised in the form of two parameters,  $S$  and  $T$ , if the new particles are heavier than half the Z-boson mass [42]. The expressions for the  $S$  and  $T$  parameters for this model have been derived in [18] and we refer to this work and [43, 44] for more discussions on the oblique parameters with vector-like fermions.

The allowed ranges for a Higgs mass of 125 GeV are  $S = 0.04 \pm 0.09$  and  $T = 0.07 \pm 0.08$  and these errors are correlated with a coefficient of 0.88 [45], forming a diagonally oriented error ellipse in the  $S$ - $T$  plane.

As discussed in the literature, the contributions to  $S$  and  $T$  can be kept within the experimental limits if the mass splitting between the components of the doublets,  $\Delta m = (y_c - y_n)v$ , is small. Hence, if the charged Yukawa couplings are large, the neutral Yukawa couplings must be large and vice versa. Also, the larger the vector-like masses are, the larger the mass splitting may be and the easier it is to respect the experimental limits (although we have found exceptions to this general rule which we will talk about more in section 4.2).

Absent signals of new charged states at the LHC create a mass limit on  $E_1$ . Motivated by discussions in [18, 19, 29] we apply a conservative lower limit on the lightest charged state of 110 GeV to ensure that current missing signals are consistent with our results, but remark that a detailed investigation of collider constraints and signals lies beyond the scope of this paper.

In our model there is no mixing between the new vector-like fermions and the Standard Model leptons. Such a set-up may arise from a gauged lepton number (as pointed out in [16, 31, 32]) and automatically avoids constraints from flavor physics and stabilises our dark matter candidate. For works that investigate models with mixing between a vector-like fourth generation and the SM fermions, see e.g. [22, 34, 36].

### 3.3 Dark Matter

The Lagrangian is expressed in the language of LanHEP [46] such that we can use micrOMEGAs [47] to calculate the relic abundance,  $\Omega h^2$ , and the spin-independent WIMP-Nucleon cross section  $\sigma^{\text{SI}}$ .

Results from LEP constrain the mass of an additional Majorana neutrino to be above 39 GeV [48]. Whereas this limit might in some cases be avoided due to the mixing of the DM candidate with singlet fields, it still serves as a good first estimate, because in these low mass regions a DM- $Z$  coupling must be present for consistent relic abundance. Hence, we show this limit as a dotted, vertical black line at 39 GeV in our plots.

Constraints arising from the dark matter sector include the relic abundance, direct searches and the invisible branching ratio of the Higgs  $\text{BR}_{\text{inv}}$ . We demand the relic density to lie in the range  $[0.1134, 0.1258]$  as has been measured by the Planck collaboration [49] and apply the strong limits on  $\sigma^{\text{SI}}$  of the XENON100 collaboration [50]. If the Higgs boson is kinematically allowed to decay into two dark matter particles, a significant contribution to  $\text{BR}_{\text{inv}}$  may arise, which is constrained by global fits as shown in references [11–13]. We will apply a rather strong limit in this work by demanding  $\text{BR}_{\text{inv}} < 0.2$ , but note that there are theoretical uncertainties involved [51].

For further discussions of dark matter with vector-like fermions we refer the reader to references [18, 24, 28, 32, 37].

### 3.4 Baryogenesis

To find out whether the model can achieve a strong first order phase transition, we evaluate the full free energy density  $\mathcal{F}$  numerically. In its complete form it is given by

$$\mathcal{F}(\phi, T) = V_{\text{SM}}(\phi) \pm \sum_i g_i V(m_i^2(\phi)) + T^4 \sum_i g_i I_{\mp} [m_i(\phi)/T] / 2\pi^2, \quad (4)$$

where the first term  $V_{\text{SM}}(\phi) = -\frac{1}{2}\mu^2\phi^2 + \frac{1}{4}\lambda\phi^4$  is the tree-level Higgs potential, the second term is the one-loop contributions with a plus for bosons and a minus sign for fermions, and the last term is the thermal corrections with the integrals  $I_{\mp}$  defined below.  $T$  is the temperature,  $g_i$  the degrees of freedom and  $m(\phi)$  the field dependent masses. Both sums run over all Standard Model particles and the new vector-like fermions. Only the  $W$  and  $Z$  bosons as well as the top quark are included from the SM particles, because other SM particles have negligible effects.

When using renormalisation conditions that do not change the tree level vacuum expectation value and the Higgs mass (which is fixed to 125 GeV in this work), the one-loop contributions to the free-energy are given by

$$V(m^2(\phi)) = \frac{1}{64\pi^2} m^4(\phi) \log m^2(\phi) + P(\phi), \quad (5)$$

with the polynomial  $P(\phi)$

$$P(\phi) = \frac{1}{2}\alpha\phi^2 + \frac{1}{4}\beta\phi^4. \quad (6)$$

Here, the coefficients are

$$\begin{aligned} \alpha &= \frac{1}{64\pi^2} \left\{ \left( -3 \frac{\omega\omega'}{v} + \omega'^2 + \omega\omega'' \right) \log \omega - \frac{3\omega\omega'}{2v} + \frac{3}{2}\omega'^2 + \frac{1}{2}\omega\omega'' \right\}, \\ \beta &= \frac{1}{128\pi^2 v^2} \left\{ 2 \left( \frac{\omega\omega'}{v} - \omega'^2 - \omega\omega'' \right) \log \omega + \frac{\omega\omega'}{v} - 3\omega'^2 - \omega\omega'' \right\}, \end{aligned} \quad (7)$$

with

$$\begin{aligned}\omega &= m^2(v), \\ \omega' &= \left. \frac{dm^2(\phi)}{d\phi} \right|_{\phi=v}, \\ \omega'' &= \left. \frac{d^2m^2(\phi)}{d\phi^2} \right|_{\phi=v}.\end{aligned}\tag{8}$$

The last part of equation (4), the thermal corrections, include the loop functions

$$I_{\mp}(x) = \pm \int_0^{\infty} dy y^2 \log\left(1 \mp e^{-\sqrt{y^2+x^2}}\right),\tag{9}$$

where  $I_-$  is the contribution from bosons and  $I_+$  from fermions.

A first indicator whether a large enough deviation from thermal equilibrium exists for baryogenesis to be possible is the ratio of the vacuum expectation value at the critical temperature,  $v_c$ , divided by the critical temperature  $T_c$  itself. If  $v_c/T_c$  is larger than one, sphaleron processes in the broken phase are suppressed and no wash-out of a baryon asymmetry can occur. In the rest of our analysis this will form our criterion whether baryogenesis can be successful.<sup>1</sup>

Note, that baryogenesis also requires a new source of CP-violation, which could arise in this model from complex Yukawa couplings. We leave an investigation of this extended parameter space open for future work and refer to reference [23] for discussions on a possible signature of these CP-phases in the diphoton decay channel of the Higgs.

It has been shown that fermions may induce a strong first order phase transition [26, 54, 55] and we refer the reader to these references for detailed discussions about the involved mechanisms, but give a short summary here for completeness.

In [54] an effective field theory approach was used to show that  $\phi^6$ -terms in the scalar potential can lead to a barrier at zero temperature. Whereas they used a scalar singlet as an example to generate these terms, one can also think of  $\phi^6$ -terms arising from fermions, such that this mechanism is applicable to fermionic extensions of the Standard Model as well. However, we do not observe a zero temperature barrier in our case, concluding that temperature corrections are crucial.

The mechanism in [55] relies on decoupling of heavy fermions from the plasma when they enter the broken phase resulting in a delay of the phase transition towards cooler temperatures and enhancing its strength in this way. Since some of our particles become lighter when they enter the broken phase, this effect is not the driving force behind our barrier.

The main effect occurring here is described in [26]. Temperature corrections can drive the effective quartic coupling  $\lambda_{\text{eff}}$  negative while  $\mu_{\text{eff}}$  becomes positive, resulting in a barrier at finite temperature. A positive  $\phi^6$  term stabilises the potential up to some energy scale.

Large Yukawa couplings necessary for the barrier intuitively stand in conflict with the oblique parameters and the dark matter sector, because large Yukawa couplings may quickly lead to an underproduction of dark matter and to a WIMP-Nucleon cross section above current exclusion limits. Hence, a detailed discussion of the model is necessary and we investigate in the following the compatibility of those constraints all together.

We used existing works in the literature and Mathematica to cross-check our numerical results.

---

<sup>1</sup>For concerns about gauge invariance of  $v_c$  and  $T_c$ , see [52, 53].

### 3.5 Diphoton Rate

Since vector-like fermions don't change the production channels of the Higgs, the excess in the Higgs diphoton channel is characterised by the ratio of the decay rates only:

$$(10)$$

The known result for the decay rate

$$\Gamma(h \rightarrow \gamma\gamma) \propto \left| A_1(\tau_W) + \frac{4}{3}A_{1/2}(\tau_t) + \frac{C^{E_1 E_1 h \nu}}{\sqrt{2}M_{E_1}}A_{1/2}(\tau_{E_1}) + \frac{C^{E_2 E_2 h \nu}}{\sqrt{2}M_{E_2}}A_{1/2}(\tau_{E_2}) \right|^2, \quad (11)$$

includes  $\tau_x = \frac{m_h^2}{4m_x^2}$  as the argument in the loop functions

$$A_{1/2}(\tau) = \frac{2(\tau + (\tau - 1)f(\tau))}{\tau^2}, \quad (12)$$

$$A_1(\tau) = -2 - \frac{3}{\tau} - \frac{3(2\tau - 1)f(\tau)}{\tau^2}, \quad (13)$$

for fermions and bosons, respectively. The function  $f(\tau)$  is given by

$$f(\tau) = \begin{cases} \arcsin^2 \sqrt{\tau} & \text{for } \tau \leq 1, \\ -\frac{1}{4} \left( -i\pi + \log \left[ \frac{1 + \sqrt{1 - \tau^{-1}}}{1 - \sqrt{1 - \tau^{-1}}} \right] \right)^2 & \text{for } \tau > 1. \end{cases} \quad (14)$$

To show the general dependence of the diphoton rate on the parameters, we show for completeness in figure ?? how  $R_{\gamma\gamma}$  behaves under a variation of  $m_\ell$  and  $y'_c$ . For a fixed  $m_\ell$  the diphoton rate becomes stronger with an increasing Yukawa coupling, and for a fixed Yukawa coupling  $R_{\gamma\gamma}$  decreases while  $m_\ell$  increases. These are the two general trends which have been discussed in the literature, see e.g. [17–23, 25, 27, 34, 35] for more discussions. In everything that follows all accepted scenarios have an enhanced Higgs diphoton branching ratio between 1 and 2.

We will now go on to present the effect of fulfilling these various criteria upon the interesting parameter values.

## 4 Results

Here we will present the application of the procedures outlined in the previous section and show how the different criteria affect the parameter space of our model.

### 4.1 Numerical Approach

To explore the parameter space we initially used a naive monte carlo scanning technique but we then moved on to a basic version of a Metropolis Hastings Monte Carlo Markov chain (MCMC) to search for good parameters more efficiently, especially to find regions with a strong first order phase transition. Note that we do not use the full power of the MCMC to obtain confidence levels as there is not a very well defined notion of priors for the parameters within a Lagrangian.

There are some plots which are the result of naive parameter scans where we vary the parameters randomly. Such plots (e.g. figure 4) will have, for example, very few points which are not

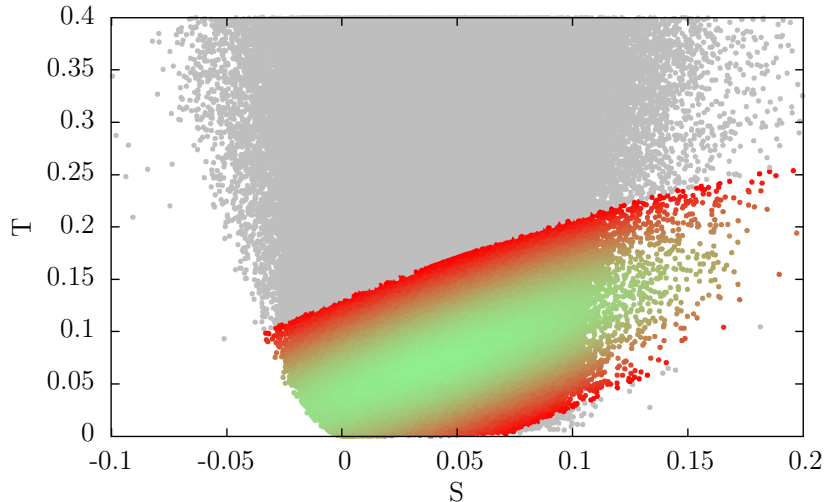


Figure 1: *The 95% confidence region of the oblique  $S$  and  $T$  parameters. Grey models which lie outside this region are rejected before any subsequent analysis.*

excluded by the XENON-100 bound on the WIMP-nucleon cross section. This told us that we had to scan the parameter space more intelligently such that we implemented the MCMC technique. Including the XENON-100 bound as a fitness criteria, the Markov chain hence concentrated on acceptable regions and the shape of the plots changed significantly (see, e.g. figure 7).

We do not claim to have made a completely comprehensive scan of the parameter space, but we have gone to some effort within the ranges described above to look for parameter combinations which satisfy all of our requirements (dark matter, baryogenesis, not too large  $S$  and  $T$  parameters) which also have Yukawa couplings as small as possible, in order to retain perturbativity.

One relic of our slightly incomplete scanning procedure is that the careful reader may be able to spot some lines on the scatter plots which are not due to any physical mechanism, but rather due to the behaviour of one of the MCMC chains as it explores the parameter range. We have tried to identify which features are physical and which are random and hopefully made this distinction clear through drawing attention to real features using colour coding and careful wording in the figure captions.

## 4.2 Electroweak Precision Oblique Parameters

In figure 1 we show the distribution of our models in the  $S$ - $T$  plane. The coloured region is part of the ellipse which represents the error on  $S$  and  $T$  and the correlation between those errors. It can be seen that the models which arise from the Lagrangian (2) generally create larger modifications to the  $T$  parameter rather than the  $S$  parameter. This is because the contribution of the mass splitting between the charged and neutral components of the doublets,  $\Delta m = (y_c - y_\nu)v$ , comes in squared for  $T$  but only enters the expression for  $S$  within a logarithm [18, 42]. See also [43, 44] for more discussions.

In some regions of the parameter space, the  $T$  parameter shows an unexpected behaviour.



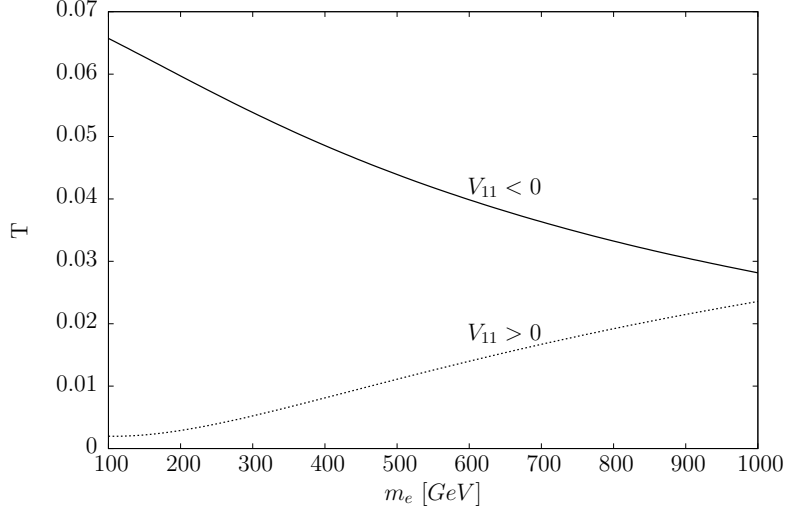


Figure 2: *The  $T$  parameter and its dependence on the vector-like mass  $m_e$  for different choices of the neutral Yukawa couplings leading to a change in sign of  $V_{11}$ .*

Whereas one would expect  $T$  to decrease when the vector-like mass terms are increased, we find that in the most general case with non-zero neutral Yukawa couplings this does not necessarily have to be the case. To understand this better, we take a closer look at the equation for the  $T$  oblique parameter [18]:

$$\begin{aligned}
4\pi s_W^2 c_W^2 M_Z^2 T = & -2 \sum_{j,k=1}^{2,4} \left( |U_{L1j}|^2 |V_{1k}|^2 + |U_{R2j}|^2 |V_{3k}|^2 \right) b_3(M_{N_k}, M_{E_j}, 0) \\
& + 2 \sum_{j,k=1}^{2,4} \text{Re} \left( U_{L1j} U_{R2j}^* V_{1k} V_{3k} \right) M_{E_j} M_{N_k} b_0(M_{E_j}, M_{N_k}, 0) \\
& + \sum_{j,k=1}^4 \left( |V_{1j}|^2 |V_{1k}|^2 + |V_{3j}|^2 |V_{3k}|^2 \right) b_3(M_{N_j}, M_{N_k}, 0) \\
& - \sum_{j,k=1}^4 \text{Re} \left( V_{1j} V_{1k}^* V_{3j} V_{3k} \right) M_{N_j} M_{N_k} b_0(M_{N_j}, M_{N_k}, 0) \\
& + \left( |U_{L11}|^4 + |U_{R21}|^4 \right) M_{E_1}^2 b_1(M_{E_1}, M_{E_1}, 0) \\
& + \left( |U_{L12}|^4 + |U_{R22}|^4 \right) M_{E_2}^2 b_1(M_{E_2}, M_{E_2}, 0) \\
& + \left( 2|U_{L11}|^2 |U_{L21}|^2 + 2|U_{R12}|^2 |U_{R22}|^2 \right) b_3(M_{E_1}, M_{E_2}, 0) \\
& - \sum_{j,k=1}^2 \text{Re} \left( U_{L1j} U_{L1k}^* U_{R2j} U_{R2k} \right) M_{E_j} M_{E_k} b_0(M_{E_j}, M_{E_k}, 0). \tag{15}
\end{aligned}$$

Here, we have  $s_W$  and  $c_W$  as the sine and cosine of the Weinberg angle and  $M_Z$  as the mass of

the  $Z$ -boson. The functions  $b_0, b_1$  and  $b_3$  are integrals defined as:

$$b_0(M_1, M_2, q^2) = \int_0^1 \log\left(\frac{\Delta}{\Lambda^2}\right) dx, \quad (16)$$

$$b_1(M_1, M_2, q^2) = \int_0^1 x \log\left(\frac{\Delta}{\Lambda^2}\right) dx, \quad (17)$$

$$b_3(M_1, M_2, 0) = \frac{M_2^2 b_1(M_1, M_2, 0) + M_1^2 b_1(M_2, M_1, 0)}{2}, \quad (18)$$

$$\Delta = M_2^2 x + M_1^2 (1-x) - x(1-x)q^2. \quad (19)$$

We observe that the 2<sup>nd</sup> and 4<sup>th</sup> term depend explicitly on the sign of the elements of the neutral mixing matrix  $V_{ij}$ , and consequently may increase or decrease the  $T$ -parameter. In figure 2 we present the different behavior of  $T$  resulting from a change in sign of the first component of the neutral mixing matrix  $V_{11}$ . For this figure we fixed the parameters as follows:

$$\begin{aligned} m' &= 200 \text{ GeV}, & m'' &= 200 \text{ GeV}, & m_\ell &= 750 \text{ GeV}, \\ m_\nu &= 100 \text{ GeV}, & Y'_c &= 1, & Y''_c &= 1, \end{aligned}$$

and chose  $Y'_n = 0.1$ ,  $Y''_n = 0$  and  $Y'_n = 1$ ,  $Y''_n = 1$  for the solid and dotted curve, respectively. The first choice leads to a negative value for  $V_{11}$  while the second one gives a positive  $V_{11}$  while all other entries of the mixing matrix keep their signs unchanged. Overall, there is one additional positive entry in  $V_{ij}$  for the second possibility which leads to the shown dependence of the  $T$  parameter on  $m_e$ .

In all the plots in the paper following this subsection, scenarios lying outside the 95% confidence region have been removed from the data.

### 4.3 Dark Matter

We extend existing discussions about dark matter in this model [18] by presenting results from an investigation of the complete parameter space performing a simple monte carlo scanning. In figure 3 we show the relic abundance and the different annihilation mechanisms that dominate during the freeze-out process. The shape is characterised by different resonances and thresholds.

At a dark matter mass of about 45 GeV and at approximately 65 GeV the  $Z$ - and  $h$ -resonances appear with a dominant decay into quark/antiquark pairs (mainly  $b\bar{b}$ ), represented by the red points. The red scenarios at masses above 170 GeV denote  $t\bar{t}$  final states. Above  $m_{\text{DM}} \approx 80$  GeV the possible annihilation into two  $W$ -bosons (and later also  $Z$ -bosons) comes along with another decrease in the relic abundance (light blue points). A similar feature is observed at the Higgs threshold at 125 GeV (dark blue points). Coannihilations with the lightest charged vector-like fermion  $E_1$  (light green) set in at approximately 100 GeV while coannihilations with the second lightest neutral state  $N_2$  (dark green) can be present at any mass range. In this and all following plots the dotted, vertical black line indicates the mass limit from LEP for an additional Majorana neutrino, see section 3.3 for more discussions on this.

We note here, that this picture can and will change when we concentrate on certain regions of the parameter space, as we will do when we discuss baryogenesis. Coannihilations, which seem to under-produce dark matter here, will become important as the dominant mechanism to set the relic abundance.

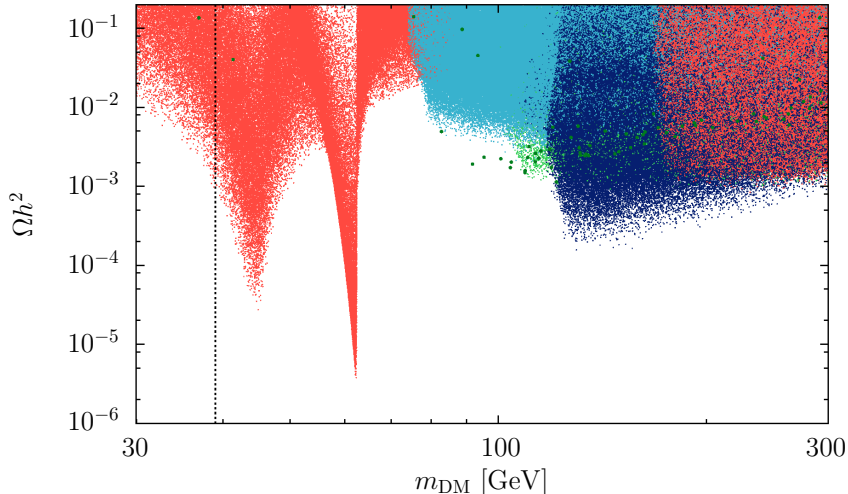


Figure 3: *The relic density and the dominant annihilation channel responsible for relic abundance. Red points represent annihilation into quark pairs, light blue points into gauge boson final states and dark blue points into a pair of Higgs bosons while light and dark green points denote co-annihilation with the lightest charged or next-to-lightest neutral fermion, respectively. In this and all following plots, the dotted vertical line shows the LEP exclusion for an additional Majorana neutrino.*

In figure 4 we present the mapping of those scenarios that fulfill the relic density condition (i.e.  $\Omega h^2 \in [0.1134, 0.1258]$ ) into the direct detection plane. We have again colour coded the diagram so it is easy to see the different sections of the diagram where different mechanisms dominate the relic abundance calculation. It is visible that direct detection limits can be avoided in the complete mass range. Since the scattering process for the WIMP-Nucleon cross section is mediated by the Higgs,  $\sigma^{\text{SI}}$  indicates the coupling of our dark matter particle to the Higgs. This is best seen at the  $h$ -resonance itself: To obtain the correct relic abundance, the resonantly enhanced annihilation rate asks for a suppressed dark matter Higgs coupling, which translates into a suppressed  $\sigma^{\text{SI}}$ .

The dark matter discussion is to some extent independent of an enhanced diphoton rate, since the latter one is solely fixed by the charged sector. However, we note that the vector mass parameter for the doublet fields,  $m_\ell$ , relates both sectors and can give rise to some correlations.

In figure 5 we show the diphoton rate in the direct detection plane with a blue color coding and can observe a general trend of a decreasing excess in the diphoton channel towards larger dark matter masses. This is because the charged states must become heavier and their contribution to the diphoton rate gets suppressed as the dark matter mass increases.

In this plot we also apply the constraint from the invisible branching ratio of the Higgs boson. Every scenario with  $\text{BR}_{\text{inv}} > 0.2$  is colored grey and therefore excluded. As expected, these scenarios populate light dark matter masses with a large WIMP-Nucleon cross section. If the LHC achieves a higher sensitivity for the invisible branching ratio, we can expect this constraint

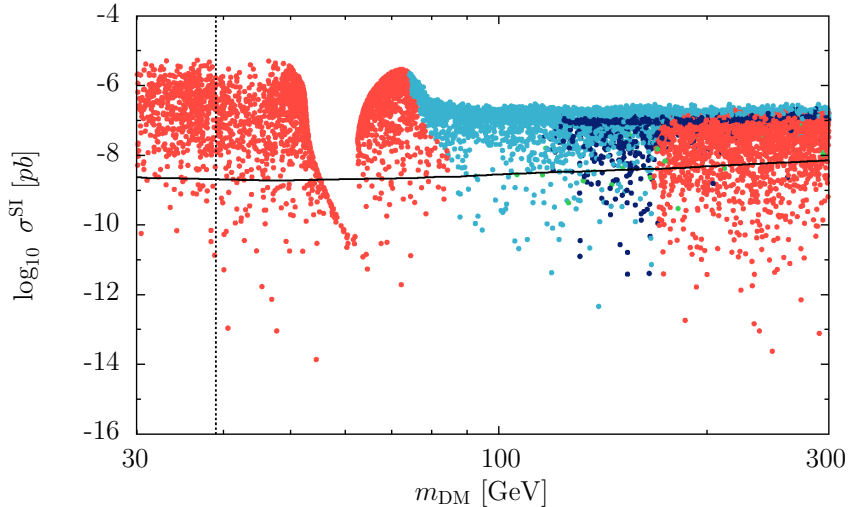


Figure 4: *WIMP-Nucleon cross section  $\sigma^{\text{SI}}$  and the dark matter mass. All points give the correct dark matter relic abundance and are colour coded by the dominant annihilation channel responsible for relic abundance. Red points represent annihilation into quark pairs, light blue points are gauge boson final states, dark blue points denote Higgs pair production while light green points denote co-annihilation with the lightest charged state. In this and all following plots the solid black line shows the XENON100 (2012) exclusion limit.*

to become more important for light dark matter masses and eventually be stronger than direct searches.

Additionally, we cross-checked the predictions of the spin-dependent WIMP-Nucleon cross section  $\sigma^{\text{SD}}$  with the current limits from the XENON100 collaboration [56], but found them to be not constraining yet. Hence, we see that we find consistent realisations of the model at every accessible dark matter mass.

#### 4.4 Baryogenesis

In order to work out if a given set of parameters leads to a strong first order phase transition, we look at the free energy equation (4) and iteratively vary the temperature until we get a phase transition. We then look for first order phase transitions and quantify the order parameter  $v_c/T_c$  to see if sphaleron processes are suppressed at and below the temperature of the phase transition, preventing washout of any baryon asymmetry.

We have analysed all the points we have found with good relic abundances in order to see which parameter sets give rise to a strong first order phase transition. In figure ?? we color code models with a smooth cross-over or a weak phase transition light-grey, and those with  $v_c/T_c > 1$  dark-grey or in a red color scale. Dark-grey points are excluded by the invisible branching ratio of the Higgs boson, whereas the red points fulfill all constraints considered in this work.

We can observe interesting behaviour at low dark matter masses. There are two dips sur-

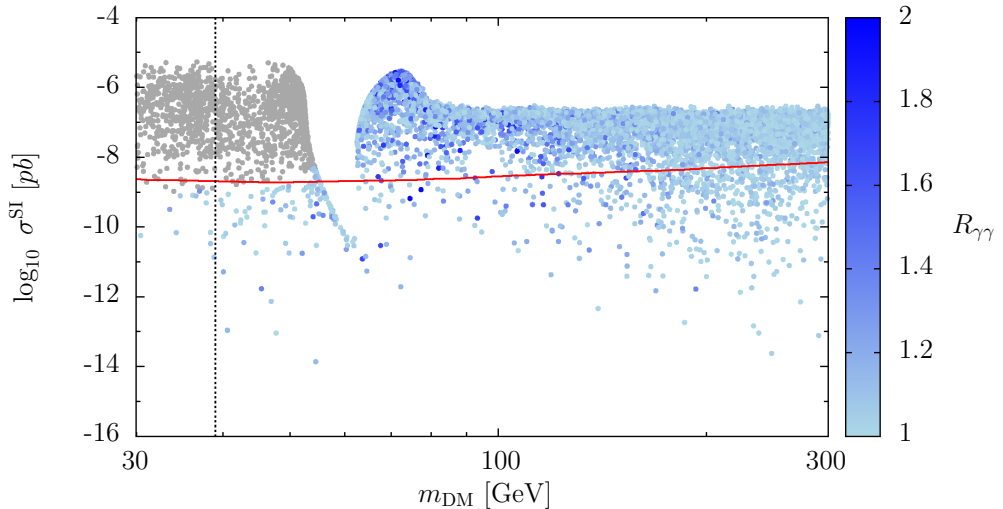


Figure 5: *WIMP-Nucleon cross section  $\sigma^{\text{SI}}$  and the dark matter mass of a general scan. The blue color indicates an enhanced Higgs to diphoton branching fraction. Grey points are excluded due to the invisible branching ratio of the Higgs.*

rounding the  $Z$ -resonance and a thin band along the  $h$ -resonance. This pattern is closely related to the constraints on the mixing of the dark matter candidate arising from demanding that we can get a strong first order phase transition. In figure 6 we show how strongly constrained the mixing becomes once we apply the baryogenesis condition  $v_c/T_c > 1$ . We show as an example the second mixing element  $V_{21}$  and note that similar plots exist for the other three elements. Again, grey points satisfy electroweak and dark matter constraints and the red points additionally the baryogenesis condition.

At the  $Z$ - resonance and at a mass around 70 GeV, one can observe that  $|V_{21}|^2$  is always non-zero if we want to get a first order phase transition. As this holds for all the other mixing elements as well<sup>2</sup>, we can understand why no suppression of  $\sigma^{\text{SI}}$  occurs. Since the direct detection process proceeds via Higgs exchange,  $\sigma^{\text{SI}}$  will be proportional to the Higgs coupling of the dark matter candidate,  $C^{N_1 hh}$ , which is given by

$$\begin{aligned} C^{N_1 hh} &= \frac{y'_n}{\sqrt{2}} (V_{11}^* V_{21}^* + V_{11} V_{21}) + \frac{y''_n}{\sqrt{2}} (V_{31}^* V_{41}^* + V_{31} V_{41}) \\ &= \sqrt{2} y'_n \text{Re}(V_{11} V_{21}) + \sqrt{2} y''_n \text{Re}(V_{31} V_{41}) \end{aligned} \quad (20)$$

For a suppressed direct detection rate, we generally need one of the mixing elements in each product to be suppressed which cannot be achieved around the  $Z$ -resonance if we demand that the vector-like fermions are important for baryogenesis.

A second thing to note in figure ?? is the tendency of smaller order parameters towards larger dark matter masses. This is again explained through approaching the decoupling limit. As all

<sup>2</sup>Of course unitarity requests some of them to be small, but around the  $Z$ -resonance they are still significantly further away from zero than in other regions.

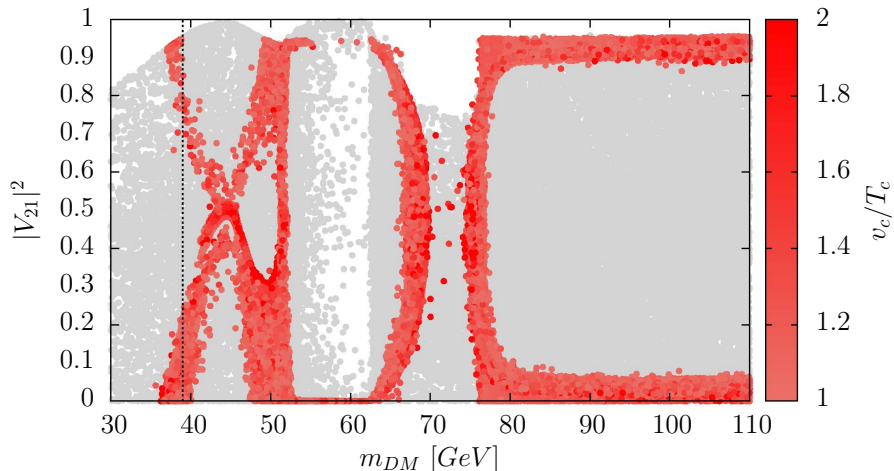


Figure 6: *The second mixing element of the dark matter candidate and the dark matter mass. Grey points fulfill electroweak and dark matter constraints, while red points additionally give a strong first order phase transition.*

masses increase, the behavior of the free energy becomes more and more standard model like and the first order phase transition gets weaker and weaker. This puts an upper limit on the dark matter candidate of around 300 GeV.

In figure 7 we look at the same data as in figure ?? but this time we colour code the annihilation channels. With this plot we can now understand the sharp edge setting in slightly below 80 GeV in figure ?. There, coannihilations of the dark matter particle with the second lightest neutral state into two  $W$ -bosons set in. The following dip at 125 GeV can now be understood with the possible annihilations processes into two Higgs bosons. We note here again, that we do expect paradoxes with figure 3 and 4 where coannihilations seemed to be unimportant for the relic abundance, because we changed our scanning procedure in such a way that we find interesting regions where baryogenesis is possible.

It is clear that we can obtain strong first order phase transitions and good dark matter abundance whilst avoiding the XENON100 bound. There are regions at particular masses below 125 GeV and for a range of masses above 125 GeV. We would like to learn more about the characteristics of the parameters which satisfy these criteria, but with nine free parameters there are many combinations which can lead to good results. There is however one feature of the parameter sets which gives rise to strong first order phase transitions, and that is that they usually require large Yukawa couplings between the Higgs and the additional fermions. In order to do that we look at a first benchmark point (BM1), which has been chosen because it satisfies all the requirements we have in terms of dark matter and baryogenesis with relatively small Yukawa couplings (relative to other parameter sets that give us baryogenesis). See table 2 for the numerical values of the parameters. We then vary the Yukawa couplings to see the effect upon the strength of the phase transition.

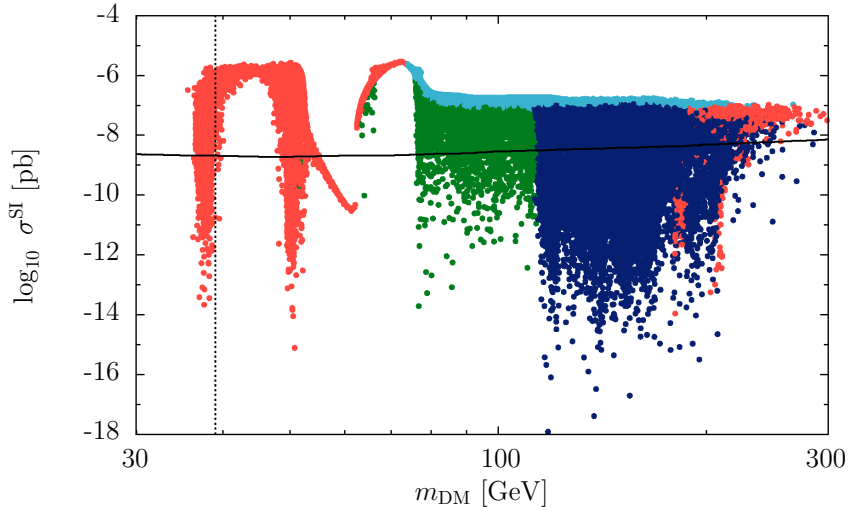


Figure 7: *WIMP-Nucleon cross section  $\sigma^{\text{SI}}$  and the dark matter mass. All scenarios produce the correct dark matter relic abundance and give a strong first order phase transition. They are colour coded by the dominant annihilation channel responsible for relic abundance. Red points represent annihilation into quark pairs, light blue points are gauge boson final states, dark blue points denote Higgs pair production and dark green points denote co-annihilation with the second lightest neutral state into a pair of quarks or  $W$ -bosons.*

Figure 8 shows the order of the phase transition as a function of the primed charged and neutral Yukawa couplings. While both Yukawa couplings increase the order of the phase transition, it seems that for the benchmark point the neutral Yukawa takes the lead role in realising baryogenesis. It becomes clear that a large ratio  $v_c/T_c$  only appears for large Yukawa couplings.

Related to this need for large Yukawa couplings, we point out that an enhanced diphoton rate is unavoidable if the fermions should cause the phase transition to be strongly first order. All simulated scenarios with  $v_c/T_c > 1$  have a minimal enhancement of  $R_{\gamma\gamma}$  of 1.1. This implies that if ATLAS and CMS will with future measurements agree on an enhanced diphoton rate, this could be interpreted as a direct connection to baryogenesis. By the same token, if both experiments agree on a Standard Model like decay rate, baryogenesis with vector-like fermions in this set-up can be excluded.

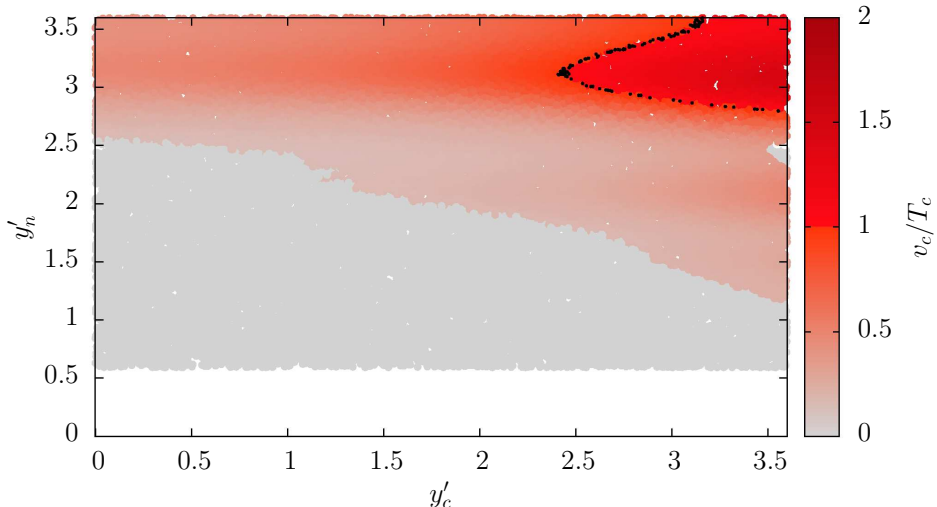


Figure 8: *The order parameter and its dependence on the primed charged and neutral Yukawa couplings. The black points have an order parameter of 1 and indicate the switchover from a weak to a strong first order phase transition. All other parameter of our benchmark point BM1 have been fixed. Note that as we vary the Yukawa couplings from the benchmark point, the other constraints ( $S$  and  $T$  parameters, dark matter relic abundance, XENON100 limit and diphoton bound) may be violated.*

#### 4.5 Vacuum Stability

	$m'$ [GeV]	$m''$ [GeV]	$m_\ell$ [GeV]	$m_\nu$ [GeV]	$m_e$ [GeV]	$y'_c$	$y''_c$	$y'_n$	$y''_n$
BM1	97.70	90.90	2172.0	124.50	482.80	2.73	2.82	2.98	2.99
BM2	869.53	236.57	2514.70	215.13	445.66	3.59	3.48	3.06	2.88

Table 2: Parameters of two benchmark points considered in the model.

The addition of exclusively new fermions to the SM renders the electroweak vacuum unstable at some scale  $\Lambda$ . If we define  $V(v) = 0$ , the scale  $\Lambda$  is set by the value of  $\phi$  for which the potential turns negative, opening up the possibility for a decay of the electroweak vacuum. We show in this section that this instability scale lies above all the fermion mass eigenvalues by explicitly plotting the zero temperature scalar potential for two benchmark points, see figure 9.

In section 3.4 we chose a benchmark point with smallest possible Yukawa couplings consistent with all our constraints. As larger values of the Yukawa couplings will generally worsen the stability of the vacuum, we additionally present a consistent realisation with Yukawa couplings very close to the perturbativity limit. In table 2 we give their specific parameters and in table 3 the mass eigenvalues as well as the instability scale. For all accepted models the instability scale is larger than the heaviest fermion mass. We note that the stabilising state(s) must appear below the instability scale, but just above the scale of the physics discussed in this paper.



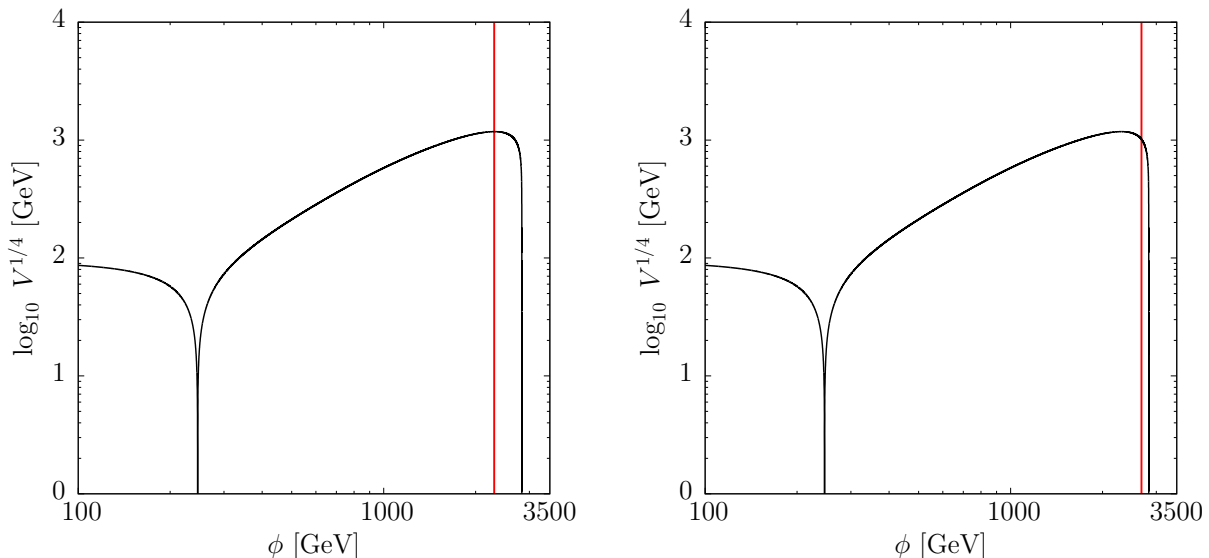


Figure 9: The zero temperature scalar potential for benchmark point 1 (left panel) and 2 (right panel). The scale of instability occurs above the largest fermion mass eigenvalue, which is indicated by a red vertical line at the corresponding energy scale.

	$m_{N_1}$ [GeV]	$m_{N_2}$ [GeV]	$m_{N_3}$ [GeV]	$m_{N_4}$ [GeV]	$m_{E_1}$ [GeV]	$m_{E_2}$ [GeV]	$\Lambda$ [GeV]
BM1	85.96	92.42	2291.24	2301.45	354.62	2300.23	2833.23
BM2	210.11	841.35	2605.85	2660.49	276.74	2683.68	2857.79

Table 3: Masses and instability scale for both benchmark points.

## 5 Discussion and Conclusions

In this paper we have investigated extensions of the standard model in the form of vector-like fermions. As has been pointed out in work [18], there is the possibility to obtain a viable dark matter candidate and the potential to increase the branching ratio of the Higgs boson decay into two photons, a channel which will be measured in more detail when the LHC starts to run again.

In section 4.3 we presented our results of a general dark matter scan and saw that this candidate can explain all the dark matter abundance in the universe in the complete mass region we investigated. We showed in figure 3 which mechanisms are the most important ones for effective annihilation in the early universe and looked at their mapping into the direct detection plane in figure 4. We saw that the invisible branching ratio of the Higgs can cut into the parameter space, but is not yet sensitive enough to be more important than limits on the WIMP-Nucleon cross section  $\sigma^{\text{SI}}$ . Models exist where  $\sigma^{\text{SI}}$  is smaller than  $10^{-50}$  cm<sup>2</sup> which presents a fresh challenge for the next generation of dark matter direct detection experiments.

We have investigated the effect upon electroweak baryogenesis of these extensions to the Standard Model in section 4.4 and showed that one can obtain a strong first order electroweak phase transition. Therefore, this kind of models enables the kind of out-of-equilibrium physics required to fulfill the Sakharov conditions. We have noted that in order to obtain successful baryogenesis, one requires relatively large Yukawa couplings between the new states and the

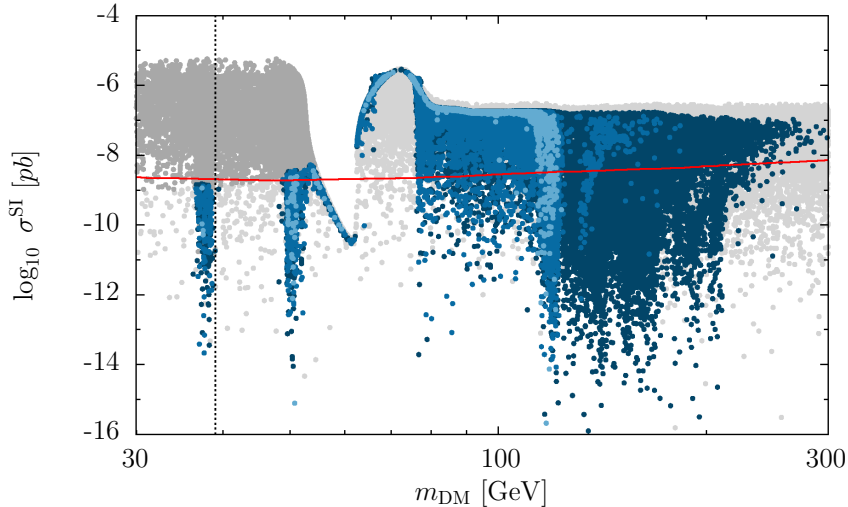


Figure 10: *WIMP-Nucleon cross section  $\sigma^{\text{SI}}$  and the dark matter mass. The solid red line is the XENON100 (2012) limit, the dotted black line shows the mass limit on a new Majorana neutrino by LEP. All scenarios give the correct relic abundance and respect electroweak precision tests. Dark grey points are, however, excluded by the invisible branching ratio of the Higgs. The blue models respect all constraints, meaning they also possess a strong first order phase transition. They are coded in three blue tones to indicate different upper limits on the diphoton excess  $R_{\gamma\gamma}$  in order to show how future measurements in the diphoton channel may affect our results. From dark to light, the corresponding upper limits on  $R_{\gamma\gamma}$  are 1.5, 1.3 and 1.2.*

Higgs, compare figure 8. These Yukawa couplings can also serve as a possible new source of CP-violation.

If we demand that this extra sector provides both our dark matter and a strong first order electroweak phase transition simultaneously, there are quite large ranges of possible dark matter masses between 39 GeV and 300 GeV with notable absences of models where the dark matter mass is around 45 GeV or 70 GeV, as can be seen in figure ?? and 10. We hence find that both these problems of modern particle physics can be addressed within this single set-up.

Once the LHC is operational again following its current shutdown, new data will clarify the Higgs to diphoton rate which will place tight constraints upon this set of models. It will be interesting to discover which regions of the parameter space will still be available if the constraints on this rate are increased.

To explore this further, we show in figure 10 regions of models that explain both dark matter and baryogenesis, colour coded according to the value of the excess in the diphoton channel. As in the rest of the paper, we show a background of light-grey points that give a dark matter candidate fulfilling the relic density condition and electroweak constraints with an excess in the diphoton channel between 1 and 2. Dark grey points are, however, ruled out by the upper limit on the invisible branching ratio of the Higgs. All blue points additionally give a strong first order electroweak phase transition and form the scenarios consistent with all our applied constraints.

The different shades of blue indicate different upper limits on  $R_{\gamma\gamma}$  ranking from 1.5 (darkest blue) via 1.3 (middle tone) to 1.2 (lightest blue). We can see that if in the future the excess in the diphoton channel consistently decreases in both experiments, scenarios at high dark matter masses will be ruled out. In those regions, all new vector-like fermions are relatively heavy and for successful baryogenesis the charged Yukawa couplings need to be close to their largest possible value still consistent with perturbativity, which comes along with a relatively large enhancement in the diphoton decay channel. Related to this we note again that all scenarios with a strong first order phase transition show an enhancement of  $R_{\gamma\gamma}$  of at least 1.1. This demonstrates how a better limit from the LHC in that channel can rule out electroweak baryogenesis within this model.

The best fitting values of the top quark mass and the Higgs mass suggest that the quartic coupling of the Higgs will become negative upon renormalisation to high energy scales, therefore rendering our current electroweak vacuum metastable [38–40]. The addition of fermions to the Standard Model in the way outlined in this paper will generically worsen this situation, such that the quartic coupling becomes negative at lower energies, potentially reducing the tunneling time from our vacuum to the true one to be comparable with the age of the Universe (as pointed out by the authors of [19]). We expect that the fact that baryogenesis requires large couplings in this extended sector would make this potential problem worse. In section 4.5 we pointed out that if the scenario set out in this work would turn out to be true, it would be a strong indication of additional particles at higher energies which would address this vacuum stability issue by adding positive contributions to the beta function for the quartic coupling.

## 6 Acknowledgments

We are happy to thank A. Joglekar, P. Schwaller, C. Wagner and R. Hogan for useful conversations. MF is grateful for funding from the UK Science and Technology Facilities Council. PG is supported by an ERC advanced Grant.

## References

- [1] S. Chatrchyan *et al.* [CMS Collaboration], Phys. Lett. B **716** (2012) 30 [arXiv:1207.7235 [hep-ex]].
- [2] G. Aad *et al.* [ATLAS Collaboration], Phys. Lett. B **716** (2012) 1 [arXiv:1207.7214 [hep-ex]].
- [3] J. H. Christenson, J. W. Cronin, V. L. Fitch and R. Turlay, Phys. Rev. Lett. **13** (1964) 138.
- [4] R. Aaij *et al.* [LHCb Collaboration], Phys. Rev. Lett. **108** (2012) 111602 [arXiv:1112.0938 [hep-ex]].
- [5] A. D. Sakharov, Pisma Zh. Eksp. Teor. Fiz. **5** (1967) 32 [JETP Lett. **5** (1967) 24] [Sov. Phys. Usp. **34** (1991) 392] [Usp. Fiz. Nauk **161** (1991) 61].
- [6] G. 't Hooft, Phys. Rev. Lett. **37** (1976) 8.
- [7] V. A. Kuzmin, V. A. Rubakov and M. E. Shaposhnikov, Phys. Lett. B **155** (1985) 36.
- [8] M. Fukugita and T. Yanagida, Phys. Lett. B **174** (1986) 45.

- [9] M. A. Luty, Phys. Rev. D **45** (1992) 455.
- [10] G. W. Anderson and L. J. Hall, Phys. Rev. D **45** (1992) 2685.
- [11] P. P. Giardino, K. Kannike, I. Masina, M. Raidal and A. Strumia, arXiv:1303.3570 [hep-ph].
- [12] J. Ellis and T. You, JHEP **1306** (2013) 103 [arXiv:1303.3879 [hep-ph]].
- [13] A. Falkowski, F. Riva and A. Urbano, arXiv:1303.1812 [hep-ph].
- [14] [ATLAS Collaboration], ATLAS-CONF-2013-012.
- [15] C. Palmer [for the CMS Collaboration], arXiv:1305.3654 [hep-ex].
- [16] P. Fileviez Perez and M. B. Wise, JHEP **1108** (2011) 068 [arXiv:1106.0343 [hep-ph]].
- [17] M. Carena, I. Low and C. E. M. Wagner, JHEP **1208** (2012) 060 [arXiv:1206.1082 [hep-ph]].
- [18] A. Joglekar, P. Schwaller and C. E. M. Wagner, JHEP **1212** (2012) 064 [arXiv:1207.4235 [hep-ph]].
- [19] N. Arkani-Hamed, K. Blum, R. T. D'Agnolo and J. Fan, JHEP **1301** (2013) 149 [arXiv:1207.4482 [hep-ph]].
- [20] L. G. Almeida, E. Bertuzzo, P. A. N. Machado and R. Z. Funchal, JHEP **1211** (2012) 085 [arXiv:1207.5254 [hep-ph]].
- [21] B. Batell, D. McKeen and M. Pospelov, JHEP **1210** (2012) 104 [arXiv:1207.6252 [hep-ph]].
- [22] J. Kearney, A. Pierce and N. Weiner, Phys. Rev. D **86** (2012) 113005 [arXiv:1207.7062 [hep-ph]].
- [23] M. B. Voloshin, Phys. Rev. D **86** (2012) 093016 [arXiv:1208.4303 [hep-ph]].
- [24] C. Arina, R. N. Mohapatra and N. Sahu, Phys. Lett. B **720** (2013) 130 [arXiv:1211.0435 [hep-ph]].
- [25] B. Batell, S. Jung and H. M. Lee, JHEP **1301** (2013) 135 [arXiv:1211.2449 [hep-ph]].
- [26] H. Davoudiasl, I. Lewis and E. Ponton, arXiv:1211.3449 [hep-ph].
- [27] W. -Z. Feng and P. Nath, Phys. Rev. D **87** (2013) 075018 [arXiv:1303.0289 [hep-ph]].
- [28] P. Fileviez Perez and M. B. Wise, JHEP **1305** (2013) 094 [arXiv:1303.1452 [hep-ph]].
- [29] A. Joglekar, P. Schwaller and C. E. M. Wagner, JHEP **1307** (2013) 046 [arXiv:1303.2969 [hep-ph]].
- [30] B. Kyae and C. S. Shin, JHEP **1306** (2013) 102 [arXiv:1303.6703 [hep-ph]].
- [31] M. Duerr, P. Fileviez Perez and M. B. Wise, Phys. Rev. Lett. **110** (2013) 231801 [arXiv:1304.0576 [hep-ph]].
- [32] P. Schwaller, T. M. P. Tait and R. Vega-Morales, arXiv:1305.1108 [hep-ph].

- [33] R. Huo, arXiv:1305.1973 [hep-ph].
- [34] R. Dermisek and A. Raval, arXiv:1305.3522 [hep-ph].
- [35] S. K. Garg and C. S. Kim, arXiv:1305.4712 [hep-ph].
- [36] K. Ishiwata and M. B. Wise, arXiv:1307.1112 [hep-ph].
- [37] K. -Y. Choi, B. Kyae and C. S. Shin, arXiv:1307.6568 [hep-ph].
- [38] J. Elias-Miro, J. R. Espinosa, G. F. Giudice, G. Isidori, A. Riotto and A. Strumia, Phys. Lett. B **709** (2012) 222 [arXiv:1112.3022 [hep-ph]].
- [39] G. Degrandi, S. Di Vita, J. Elias-Miro, J. R. Espinosa, G. F. Giudice, G. Isidori and A. Strumia, JHEP **1208** (2012) 098 [arXiv:1205.6497 [hep-ph]].
- [40] D. Buttazzo, G. Degrandi, P. P. Giardino, G. F. Giudice, F. Sala, A. Salvio and A. Strumia, arXiv:1307.3536 [hep-ph].
- [41] G. Belanger, N. D. Christensen, A. Pukhov and A. Semenov, Comput. Phys. Commun. **182** (2011) 763 [arXiv:1008.0181 [hep-ph]].
- [42] M. E. Peskin and T. Takeuchi, Phys. Rev. D **46** (1992) 381.
- [43] F. del Aguila, J. de Blas and M. Perez-Victoria, Phys. Rev. D **78** (2008) 013010 [arXiv:0803.4008 [hep-ph]].
- [44] G. Cynolter and E. Lendvai, Eur. Phys. J. C **58** (2008) 463 [arXiv:0804.4080 [hep-ph]].
- [45] J. Beringer *et al.* [Particle Data Group Collaboration], Phys. Rev. D **86** (2012) 010001.
- [46] A. Semenov, arXiv:1005.1909 [hep-ph].
- [47] G. Belanger, F. Boudjema, P. Brun, A. Pukhov, S. Rosier-Lees, P. Salati and A. Semenov, Comput. Phys. Commun. **182** (2011) 842 [arXiv:1004.1092 [hep-ph]].
- [48] C. Amsler *et al.* [Particle Data Group Collaboration], Phys. Lett. B **667** (2008) 1.
- [49] P. A. R. Ade *et al.* [Planck Collaboration], arXiv:1303.5076 [astro-ph.CO].
- [50] E. Aprile *et al.* [XENON100 Collaboration], Phys. Rev. Lett. **109** (2012) 181301 [arXiv:1207.5988 [astro-ph.CO]].
- [51] A. Djouadi and G. Moreau, arXiv:1303.6591 [hep-ph].
- [52] H. H. Patel and M. J. Ramsey-Musolf, JHEP **1107** (2011) 029 [arXiv:1101.4665 [hep-ph]].
- [53] C. L. Wainwright, S. Profumo and M. J. Ramsey-Musolf, Phys. Rev. D **86** (2012) 083537 [arXiv:1204.5464 [hep-ph]].
- [54] C. Grojean, G. Servant and J. D. Wells, Phys. Rev. D **71** (2005) 036001 [hep-ph/0407019].
- [55] M. S. Carena, A. Megevand, M. Quiros and C. E. M. Wagner, Nucl. Phys. B **716** (2005) 319 [hep-ph/0410352].
- [56] E. Aprile *et al.* [XENON100 Collaboration], arXiv:1301.6620 [astro-ph.CO].